No. 132/24, 35–56
ISSN 2657-6988 (online)
ISSN 2657-5841 (printed)
DOI: 10.26408/132.03

Submitted: 07.06.2024
Accepted: 23.08.2024
Published: 18.12.2024

APPLICATION OF THE VIVALDI ANTENNA IN A LINEAR ANTENNA ARRAY FOR RADAR SYSTEMS

Marian Wnuk
Military University of Technology, gen. Sylwestra Kaliskiego 2, 00–908 Warsaw 46, Poland, ORCID 0000-0003-4576-4023, e-mail: marian.wnuk@wat.edu.pl

Abstract: The article presents a new broadband TSA antenna with a widening aperture, which is to be the basic radiating element in a multi-element antenna. The TSA antenna is characterized by a low-value standing wave ratio (SWR) covering the widest possible frequency band while maintaining a symmetrical and directional radiation pattern. The design was created using the WIPL-D computer program. This program enabled a computer simulation and the selection of the final solution. The "output" model is a radiator powered by a half-wave dipole. The results include the computer simulations of multi-element antennas, as well as the physical measurements carried out in an anechoic chamber for various configurations of antenna arrays. The discussion includes a number of significant problems that arise in the construction of antenna arrays, their various solutions, while the method of their power supply, as carried out in this paper, requires obtaining a bandwidth of 700–800 kHz for the SWR < 2 criterion (for radar applications this criterion is the more stringent SWR < 1, 3).

Keywords: tapered slot antennas, antenna array, Vivaldi antennas.

1. INTRODUCTION

The increasing use of radio systems in various areas of life has resulted in increasingly higher requirements for antenna systems. In particular, new solutions related to antenna technology focus on reducing the dimensions of the antennas, obtaining a wide operating band and ensuring the ability to scan a wide range of angles. Tapered Slot Antennas (TSA), also known as Vivaldi antennas, have been identified as a potential candidate for wide-band scanning, with the ability to scan over a wide range of angles in phased array applications. These antennas already have supporters since their introduction by Lewis in 1974, where broadband was recognized as their primary advantage. The fact that these antennas are the object of great interest means that there are already a considerable number of variants of these antennas. The use of TSA antennas consisting of a double-sided foiled dielectric laminate, which had a number of disadvantages, has been abandoned:

- lowering the energy efficiency of the antenna;
- high cost of laminate, especially high-quality laminate;
- lowering the directionality of the antennas containing dielectric elements;
- in large antenna arrays, harmful excitation may occur along with hard to eliminate surface waves and radiators without dielectric elements, which allows for partial elimination of defects occurring when using a dielectric laminate.

As millimeter wave and microwave phased array antennas are increasingly important components of many applications, including satellite and terrestrial communications, radars, vision systems, etc., it is interesting to increase the efficiency of using Vivaldi antennas due to their usefulness in broadband phased arrays. Single and double polarized antenna arrays with elements in the form of TSA antennas are becoming a field of extensive analysis using effective numerical algorithms. Phased antenna arrays are attractive for applications that require fast beam sweeps or multiple simultaneous beams. Recent improvements in digital receivers and signal processing make phased arrays especially attractive for broadband sweeps over a large number of sectors. Proper array designs provide a large number of simultaneous beams for signals of different band frequencies, limited mainly by digital processing capacity. To accomplish this, the receiving apparatus is a compromise of elements exhibiting good input impedance and wide radiation characteristics over the entire operating band. In addition, these characteristics are maintained by the presence of adjacent element fasteners. Currently, TSA antennas are the only components that meet all these requirements, and they can be placed close enough in the array to avoid high levels of sidelobes in two or more octaves in the band.

Particularly interesting are the use of TSA antennas as radiators in 3D radar arrays. Their advantages may form a perspective on the solutions used so far. Due to a wide use of radio systems in various areas of life, increasingly higher requirements are placed on the antenna systems. In particular, new solutions related to antenna technology focus on reducing the size of the antennas, obtaining a wide operating band and ensuring the possibility of scanning over a wide range of angles.

The TSA [Kołosowski, Wnuk and Jeziorski 2003], or widening slot antennas, also known as Vivaldi antennas [Schaubert 1985], have been recognized as a potential candidate for wide band operation, with the ability to scan over a wide range of angles. These antennas have had their advocates since their introduction by Lewis in 1974, and their primary advantage is broadband. The fact that these antennas are of great interest means that there are already a considerable number of variants in the design of these antennas.

At present, the use of TSA antennas consisting of a double-sided foiled dielectric laminate is being abandoned, meaning radiators without dielectric elements are used, with a partial elimination of the drawbacks occurring in the use of a dielectric laminate. Since phased antenna arrays of millimeter waves and microwaves are becoming increasingly more important elements of many

applications, including satellite or terrestrial communications, radars, vision systems, etc., an interesting issue is increasing the efficiency of using the Vivaldi antennas [Gibson 1979; De Oliveira et al. 2015], due to their usefulness in broadband phased arrays.

Single and double polarized antenna arrays with TSA antenna elements [Chio, Schubert and Holter 2000] are becoming a field of extensive analysis using efficient numerical algorithms. Beveled antenna arrays are attractive for applications requiring fast beam scanning or multiple simultaneous beams. Recent improvements in digital receivers and signal processing make especially phased arrays attractive for wideband scanning in a large number of sectors. Proper pattern designs provide a large number of simultaneous beams for signals with different band frequencies, limited mainly by digital processing capacity. To achieve this, the receiving apparatus is a compromise of elements showing good input impedance and broad radiation characteristics throughout the entire operating range. Currently, TSA [Kolundzija] antennas are the only components meeting all these requirements and they can be placed close enough in the array to avoid high side lobes in two or more octaves per band. The use of TSA [Greenberg and Virga Hammond 2003] antennas as radiators in antenna arrays of three-coordinate radars may eventually be particularly interesting.

The element that included in the pattern is schematically shown in Figure 1. It is a metal element consisting of two planes with a cut-out slot, where the planes are interconnected by the side walls and the bottom wall [Frane and Leggetter 1987].

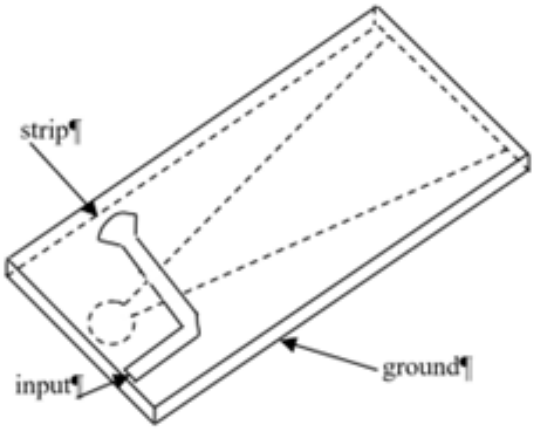

Fig. 1. Model of the asymmetrical TSA antenna used for array operation

2. VIVALDI ANTENNAS

The class of Vivaldi antennas are constructed as a combination of many conductive layers arranged on at least one layer of the substrate [Prasad and Mahapatra 1983]. The conductive layers are arranged to create an expanding gap. The gap widens from the closed end to the open end. An important issue is the shape of the slit, as initially it was designed as an exponential curve while now it is increasingly often designed as a hybrid curve. It includes many auto-like curve segments, because as the curve expands, each curve segment is scaled by the scaling factor and joins its wider end to an adjacent curve segment. The antenna array thus becomes much broader than the previous exponential slot shape arrays.

The Vivaldi antenna element was first extensively described by [Gibson 1979]. The original Vivaldi antennas were slit-widening antennas that had an exponential shape[Li et al. 2013]. They were constructed using conventional microwave lithography – a thin conductive film technique on substrates having a high dielectric constant – such as alumina. Gibson's work then focused on constructing more robust Vivaldi antennas and this led to the use of non-alumina ceramic substrates having high or low dielectric constants, e.g. plastics. Copper-clad plastics such as PTFE, RT / duroid (exhibiting a range of properties, $\varepsilon_r = 2.2$ or 2.94) or Kapton ($\varepsilon_r = 3.5$) are now widely used as the ease of construction and price are important. Conductive layers can also be made of other conductors, including gold and gold-plated copper. The exponential slit spread shape was originally used to meet the requirements of a fixed beamwidth antenna that could operate in the microwave frequency range between 2 and 20 GHz.

In theory, a Vivaldi antenna should radiate radio frequency magnetic waves of a given wavelength when the width of the widening slit (at right angles to the axis of symmetry) is approximately half the wavelength [Mikhnev and Vainikainen 2006]. The physical performance of conventional antennas is defined by a number of complex factors. It has been experimentally established that the conventional exponential extension shape of the Vivaldi antenna shows poor performance at ultra-wide bandwidths. The acute radiation properties of the exponential extension rapidly deteriorate beyond the characteristic range [Langle, Hali and Newman 1996].

A perfect antenna would radiate electromagnetic waves of a given frequency at some point along the center line of the slit for which the width of the widening slit would be half the wavelength of the given frequency. In a real application, as a given frequency increases, the radiation point moves towards the closed end of the aperture. As the slit narrows, the gradient of the exponential edge of the slit decreases towards the closed end and becomes too shallow to radiate effectively. As the given frequency decreases, the radiation point moves towards the open end of the slit, the slit becomes wider, the gradient of the exponential curve increases and becomes too steep to radiate effectively [Noronha et al. 2003].

For TSA antennas, there are many possibilities of modelling their structures, which is why they are the subject of many studies aimed at finding the best solutions to optimize their parameters and eliminate the disadvantages of earlier models.

2.1. Vivaldi antenna gap analysis

The analysis of the TSA antenna consists of two steps and is performed for an unbalanced antenna. In the first step, the electric field in the narrowed gap is analyzed. In the second step, the far radiation zone is analyzed, which is caused by an equivalent magnetic current in the aperture obtained with the use of appropriate Green functions [Gazit 1998]. The presence of the dielectric is taken into account in the calculations in the first step, but not in the second. The effects at the ends of the structure are introduced by adding a backward wave. Under these conditions, the task reduces to finding the field distribution for the case of a narrowed slit line. To achieve this, a continuous slit is approximated by a number of sections of a uniformly wide slit. The slot is divided into sections [Gibson 1979], in which the slot edges are parallel to each other with the relationship that in each section the distance between the edges is different (Fig. 2). The slit and characteristic impedance changes from section to section, according to the slit width.

The second step in the analysis is to determine the radiated field of the narrowed slit using the field distribution determined in the first step. The antenna tips induce currents that must be included in the analysis [Zhao 2004]. The near zone scattering is included in the calculations [Prasad and Mahapatra 1983] by treating the slit as radiation propagating in the presence of a conducting half-plane.

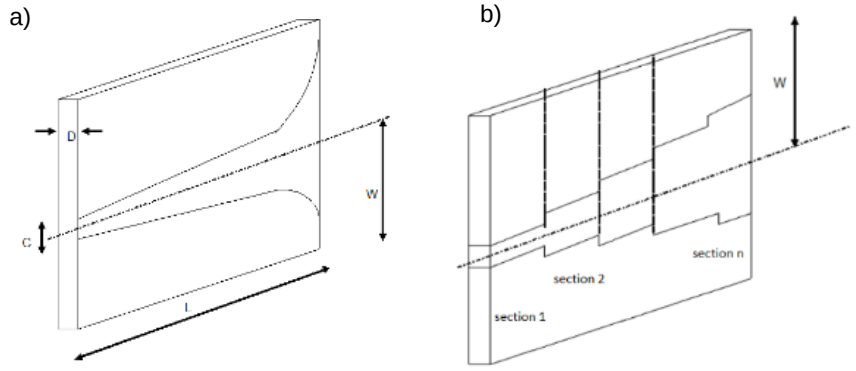

Fig. 2. Vivaldi antenna model used to build the model and mathematical description: a) actual dimensions, b) step approximation

2.2. Mathematical description of phenomena occurring in the antenna

The slit of wavelength λ_o, the characteristic impedance Z_o, and the electric field of a single section of the slit were determined using the spectral Galerkin technique. The transverse field of [Li et al. 2013] the slit E_z^s in a single section is described:

$$E_z{}^s(z) = \left(\frac{2}{\pi W}\right)\sum_{n=1}^{M_z} a_n \frac{T_{2(n-1)}\left(\frac{2z}{W}\right)}{\sqrt{1-(\frac{2z}{W})^2}} = \sum_{n=1}^{M_z} a_n e_n{}^z(z) \tag{1}$$

where:

$Tn(\bullet)$ – a Chebyshev polynomial of the first kind of order *n*,
E_z^s – an even function z which is the field configuration for the line.

The basic functions were selected to meet the boundary conditions on the edge. The Fourier transform of a basic function can be represented as:

$$\tilde{e}_n{}^z(\alpha W) = (-1)^{n+1} J_{2(n-1)}(\frac{\alpha W}{2})) \tag{2}$$

where α – the transformed variable.

The power P_f, the characteristic impedance Z_o and the electric field of the gap E_z^s are related:

$$P_f = \frac{|V_o|^2}{Z_o} = \frac{|\tilde{E}_z(0)|^2}{Z_o} \tag{3}$$

where $E_z(\alpha)$ – the Fourier transform of E_z^s.

For the above selection of the fundamental function, $E_z(0) = a_1$, where a_1 is the amplitude of the first transverse basic function. The steady stream of power along the aperture implies that:

$$\ldots = \frac{|a_1{}^{i-1}|}{\sqrt{Z_0{}^{i-1}}} = \frac{|a_1{}^i|}{\sqrt{Z_0{}^i}} = \frac{|a_1{}^{i+1}|}{\sqrt{Z_0{}^{i+1}}} = \cdots = \sqrt{P_f} = const. \tag{4}$$

where the superscripts indicate the section number. We re-normalize the coefficients in (1) and in (4) and insert the wave propagating phase factor. The area of the *z*-oriented slit in the i-th section is given:

$$E_z{}^i(x', z') = e^{jk_x{}^i x'}\left(\frac{2\sqrt{Z_0{}^i}}{\pi W^i}\right)\sum_{n=1}^{M_z^i} \frac{a_n^i T_{2(n-1)}(\frac{2z'}{W^i}0}{\sqrt{1-(\frac{2z'}{W^i})^2}} = e^{jk_x^i x'} E_a^i(Z') \tag{5}$$

where k_x^i – the propagation constant in the i-th section which must be determined by a numerical search like $E_z^i(x',Z')$, which is a uniform slit line form corresponding to the i-th section [Chen et al. 2005].

The coefficient neither in the i-th section is normalized such that $a_1^i = 1$ and all other coefficients of the mode are defined in the periods a_1^i. The equivalent magnetic gap currents are proportional to (5) and are radiated at the presence of a conductive half-plane. The Green function of this half-plane explains the near zone scattered by the metallic edge of the TSA antenna but ignores the effects of the thin substrate. The far zone with a slight slit located on the (x', z') conducting half-plane is described:

$$e_\theta(\theta,\phi) = |\sin\varphi| e^{j\pi/4} F(\vartheta) e^{+jk_0\left(x'\sin\theta\cos\phi + z'\cos\theta\right)} + \frac{\sin\left(\frac{\varphi}{2}\right) e^{-j\left[\pi/4 + k_o\left(x'\sin\theta - z'\cos\theta\right)\right]}}{\sqrt{\pi k_o x'\sin\theta}} \tag{6}$$

where $\nu = k_o x' \sin\theta(1 + \cos\phi)$.

$F(\bullet)$ is the Fresnel integral defined as:

$$(\vartheta) = \int_0^\nu \frac{e^{-jt}}{\sqrt{2\pi t}} dt \tag{7}$$

Antenna radiation is obtained by summing the components of all sections. As a result of the transformations, we obtain:

in plane E:

$$E_\theta^i(\theta) = \tilde{E}_a^i\left(k_o W^i \cos\theta\right)\sqrt{\frac{2}{\sin\theta}}\left[e^{-jk_0 c^i{}_L}\left\{\frac{F*\left(u_h^i\right) - F*\left(u_l^i\right)}{\sqrt{c^i - \sin\theta}}\right\} + \Gamma e^{jk_0 c^i{}_L}\left\{\frac{F\left(\bar{u}_h^i\right) - F\left(\bar{u}_l^i\right)}{\sqrt{c^i + \sin\theta}}\right\}\right] \tag{8}$$

in plane H:

$$E_\theta^i(\varphi) = \tilde{E}_a^i(0)[\{\frac{e^{-jk_0 c^i{}_L}}{(c^i + \cos\varphi)}\{\sin\varphi\left[F\left(p_h^i\right) - F\left(p_l^i\right)e^{j\vartheta^i}l\right] + + \sin\left(\frac{\varphi}{2}\right)\sqrt{2(c^i - 1)}\left[F*\left(q_h^i\right) - F*\left(q_l^i\right)\right]\} - \Gamma\frac{e^{jk_0 c^i{}_L}}{(c^i - \cos\varphi)}\sin\varphi\, F\left(p_h^i\right)e^{-j\tilde{\vartheta}_h^i} - F\left(p_l^i\right)e^{-j\tilde{\vartheta}_l^i}] - \sin\left(\frac{\varphi}{2}\right)\sqrt{2(c^i + 1)}\left[F\left(\bar{q}_h^i\right) - F\left(\bar{q}_l^i\right)\right]\} \tag{9}$$

where:

$c^i = (\lambda_o/\lambda')$ i-this section
$k_o = 2\pi/\lambda_o$
$u_h^i = k_o x_h^i (c^i - \sin\theta)$
$v_h^i = k_o x_h^i (c^i + \cos\phi)$

$q_h^l = k_o x_h^i (c^i - 1)$
$p_h^i = k_o x_h^i (1 + cos\phi)$
x_l^i, x_h^i, are the lower and higher coordinates of the next *i*-th sections.

$F(\bullet)$ is the Fresnel integral as defined in (5) and the asterisk (*) indicates the complex conjugation.

The contribution of the reverse traveling wave on the aperture with the relative amplitude Γ is also included in the above expressions.

$\tilde{\tilde{E}}_a^i(\bullet)$ is specified for (1), (2), and (5).

3. COMPUTER SIMULATIONS AND THEORETICAL CALCULATIONS OF SIMPLE ARRAY CHARACTERISTICS

3.1. Characteristics of a single item used to work in a pattern

The search for the best solution as to the shape of the slot and the power element was carried out for the criterion of obtaining the widest possible operating band, taking into account the condition of the standing wave ratio, the value of which was defined as SWR < 2, taking into account the use of TSA antennas in radar technology, tightening of this criterion was applied to SWR values < 1.3. Based on the simulations, the best results were obtained for the shape of the slot with elements of parallel lines and for the power supply in the form of a half-loop, as shown in Figure 3.

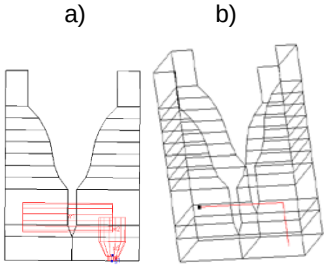

Fig. 3. The appearance of an element designed to work in a pattern in the WIPL-D program

Figure 4 shows a graph of the standing wave coefficient obtained as a result of the simulation of the designed model with elements of a parallel line: The chart shows that the antenna operating band for the SWR < 2 criterion starts at approx. 2.22 GHz and ends at approx. 3.22 GHz, which gives a working bandwidth of approx. 1.0 GHz. The percentage of the work band is about 36.76%.

On the other hand, if we consider the SWR < 1.3 criterion, which is marked with a red line on the graph, the simulated element's operating bandwidth ranges from 2.43 GHz to 3.07 GHz, which gives it a width of approx. 0.640 GHz. The percent of the work band is 23.27%.

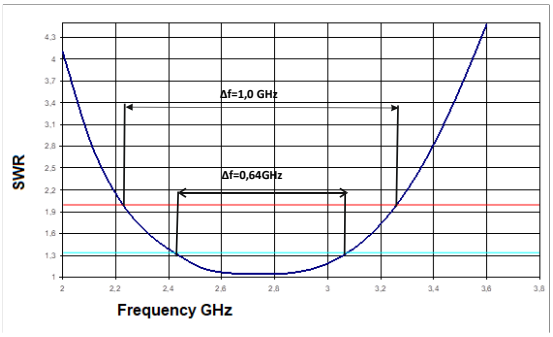

Fig. 4. Characteristics of the SWR coefficient obtained from the simulation

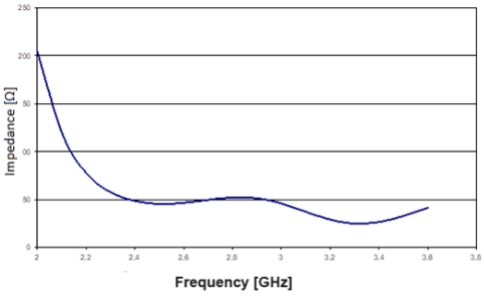

Fig. 5. Characteristics of the antenna input impedance obtained from the simulation

Figure 5 shows the characteristics of the input impedance, as we can see in the operating band that it is relatively stable, and its values show slight deviations from the value of 50 Ω.

Figure 6 shows the radiation characteristics of an element with parallel lines for three different frequencies. Symmetrical characteristics were obtained, for which the gain at all tested frequencies reached a similar value of approx. 5.71 dB. The main lobe opening is the highest for the upper frequency of the operating band, and the lowest for the lower frequency, but it is paid for with a high level of side and back lobes. Taking all these conditions into account, we obtained the best radiation characteristics parameters for the central frequency of the operating band.

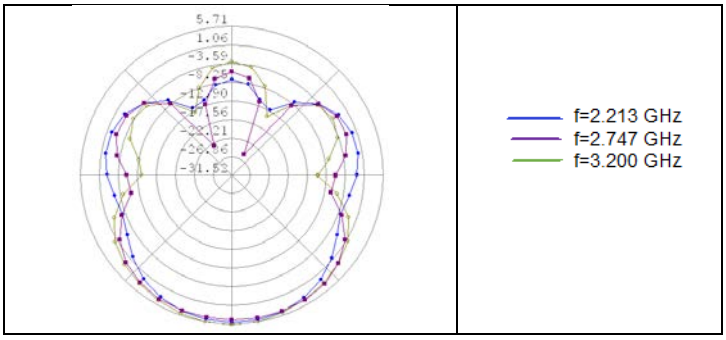

Fig. 6. The radiation pattern of a single element obtained from the simulation

3.2. Simulations of antenna arrays made using Vivaldi technology

The available version of the WIPL-D program does not allow for the simulation of complex patterns, it is related to the limitation imposed on the number of introduced unknowns. A single element that was presented earlier has 289 unknowns, while 500 such unknowns can be entered into the program. The elements that were used had the same dimensions as the power supply; however, the shape of the slot was significantly simplified, which could affect the parameters of matching this element. The performed simulations were aimed at presenting the influence of the number of elements and the distance between them on the radiation characteristics of antenna arrays [Wnuk 2022]. The differences in the shape of the slit of the simulated element and the element proposed to work in the pattern are shown in Figure 7.

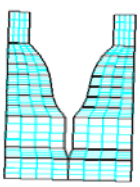

Element with a slot with elements of parallel lines

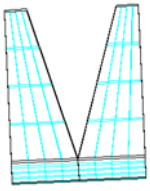

Element used to simulate the pattern operation

Fig. 7. Shape of the radiating element

3.3. Effect of changes in the distance between elements on the radiation characteristics of the pattern

Subsequent simulations were performed for two elements, and the analysis covered the influence of the positioning of the two elements in relation to each other along with the change in the distance between them on the radiation characteristics of the

array [Langley, Hali and Newman 1996; Slimi et al. 2022]. We considered two cases, and in the first the elements were located so that they had a common axis, adjacent to each other through the side walls. The simulations were performed for different distances between the elements. These distances reached the maximum value of λ, which for the central frequency of the 2.8 GHz operating band means a length of 10.7 cm. The arrangement of the elements is presented in Figure 8.

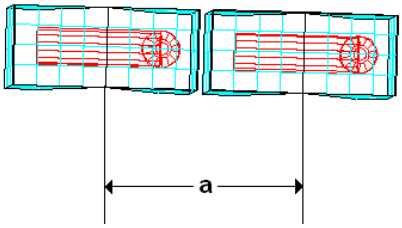

Fig. 8. Scheme of positioning of TSA antennas to simulate the effect of mutual spacing of elements on radiation characteristics

The results of the simulations are presented in Figure 9. They were carried out consecutively for a = 0.61λ; 0.71λ; 0.81λ; 0.91λ; and 1,0λ which gives respectively a = 6.42; 7.49; 8.56; 9.63 and 10.7 cm. As can be easily seen, the results for all the distances except 0.6λ are similar. In our case, this means that the characteristics achieve a similar directional gain of about 8 dB, as well as a very similar opening of the main lobe. The radiation of the side lobes and back lobes reaches quite high values, and already at a distance equal to the wavelength they reach a level equal to the radiation level of the main lobe. Significantly different simulation results were achieved for a distance of 0.6λ, the main leaf width at a level of 3 dB reaches approx. 65°, and its radiation level reaches 8.53 dB.

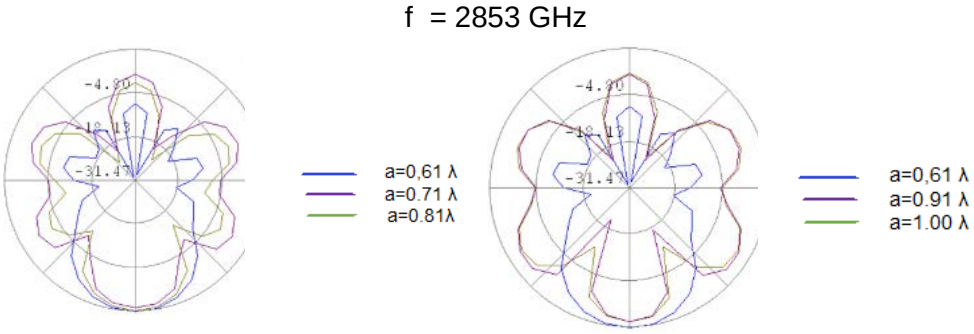

Fig. 9. The radiation characteristics obtained from the simulation showing the influence of the mutual position of the elements for f = 2853 MHZ

In this case, we also observe the lowest level of both side lobes and back lobe, which reach a value of approx. -10 dB. In the second simulated variant, the elements were positioned as in Figure 10, i.e. the adjacent walls were walls with a cut-out slot, and the impact was tested of the changes in the distance between these elements on the radiation characteristics of the array.

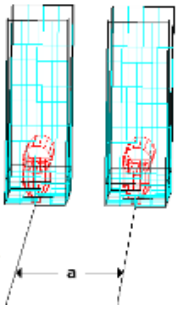

Fig. 10. Scheme of TSA antennas alignment to simulate the impact of the mutual spacing of elements on the radiation characteristics

Simulations for this configuration of the setting of radiating elements were performed for a = 0.41λ; 0.51λ; 0.61λ; 0.71λ; 0.81λ; 0.91λ; and λ, which gives respectively a = 4.28; 5.35; 6.42; 7.49; 8.56; 9.63 and 10.7 cm, as shown in Figure 11. As the simulation results show, the change in distance for such an arrangement of elements does not have a significant impact on the radiation characteristics. For all simulated distances a similar directional gain of 8.18 to 8.38 dB was achieved, while the width of the main lobe is similar at all distances and amounts to approx. 120°. We see the only changes in the radiation level of the side lobes and the back lobe, the lowest value of which is 0.4λ and increases with increasing distance between the elements.

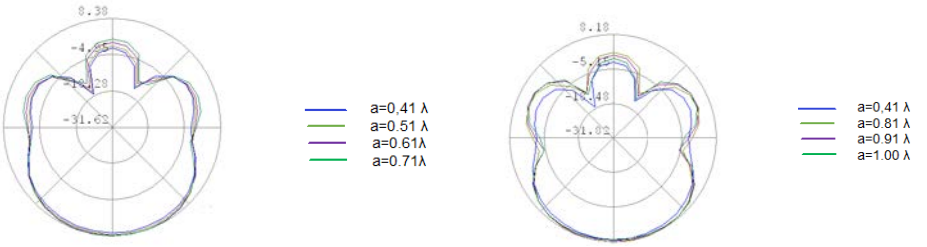

Fig. 11. The radiation characteristics obtained from the simulation showing the influence of the mutual position of the elements for f = 2853 MHZ

4. DESIGN AND MEASUREMENT OF THE CHARACTERISTICS FOR THE ANTENNA ARRAY OF TSA ANTENNAS

4.1. Characteristics of the elements included in the antenna array

The element that was used to work in the pattern is shown in Figure 12, it is the implementation of the project prepared in the WIPL-D program as the element for which the best parameters were obtained during the simulations. The shape of the slot includes elements of parallel lines, and the exact structure and dimensions of the radiating element are shown in Figure 13. A half-loop in the form of a brass rod with a diameter of 12 mm [Chen et al. 2005; Wnuk 2022] was chosen as the actuating element. A significant problem was its fastening, which was solved by the use of a dielectric support placed in the center of the radiating element aperture [Zhao 2004].

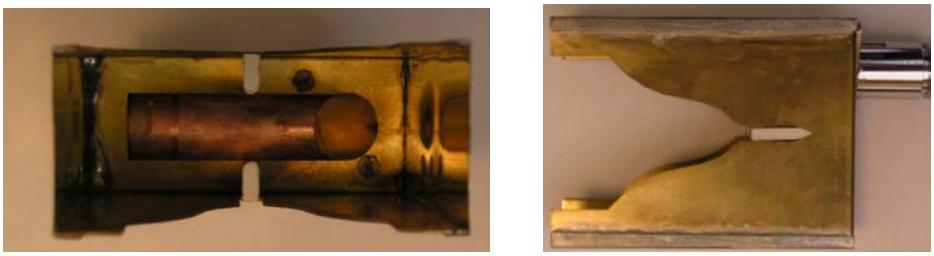

Fig. 12. Top and side view of a single element

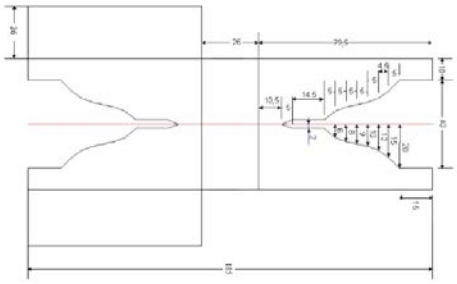

Fig. 13. Dimensions of the radiating element [cm]

The measurements of the standing wave coefficient [Noronha et al. 2003] of the radiating element allowed the determination of its operating band for both the SWR < 2 and SWR < 1.3 criteria.

The measurement results are shown in Figure 14, and it defines that:

- working band: 0.855 [GHz] for SWR < 2 (2380–3235);
- operating bandwidth: 0.520 [GHz] for SWR < 1.3 (2550–3070);
- minimum SWR value: 1.055 for the frequency of 2755 [MHz];
- frequency response for SWR: < 2.0 30.45%;
- frequency response for SWR: < 1.3 18.53%.

Figure 14 shows the radiation pattern of a radiating element for the center frequency of the operating band.

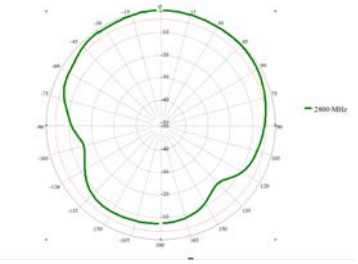

Fig. 14. Element radiation pattern for f = 2800 MHz with vertical polarization

4.2. Pattern construction

Power distribution is carried out in a designed pattern through a power divider by M / A-COM. With the co-phase excitation of all sources, the direction of the maximum radiation is perpendicular to the planes of the system [Valderas et al. 2006]. In the radiation pattern, there are two identical cigar-shaped main radiation beams. In order to reduce this effect and obtain a unidirectional characteristic, the created pattern was placed on a flat screen [Kołosowski, Wnuk and Jeziorski 2003].

The effect of the screen can be taken into account using the specular reflection method. By changing the phases of the currents in the sources, it is possible to change the position of the main beam of radiation in space. The final effect of the array structure is shown in Figure 15, where we can see the dimensioned screen and the distances between the elements in the array and the physical execution of the antenna array on the screen with the attached power distribution circuit.

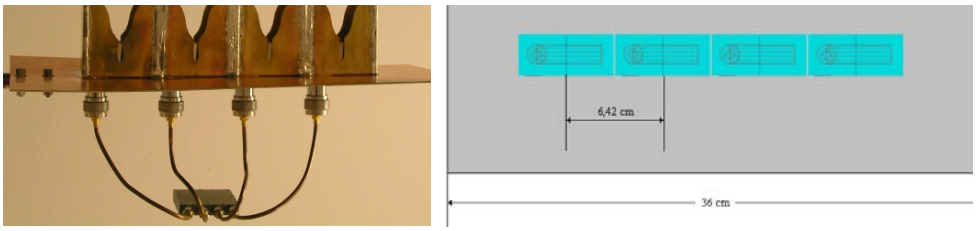

Physical implementation Dimensions of the tested pattern

Fig. 15. Dimensions of the tested pattern and its physical implementation

4.3. Measurement of coupling between two elements of the TSA antennas operating in an array

In order to measure the parameters of the antenna array, automated measuring stations were used. They were used to measure the standing wave coefficient, the S_{21} coefficient and the radiation pattern of the array. The measurements were carried out in an anechoic chamber in the far zone. The result was measuring one of the coefficients of scattering matrix S21 between two elements intended to work in the array. S_{21} is the wave transmission coefficient between the second and the first element. This coefficient gives us in decibels the degree of isolation between the gates of two elements. Measurements were made for different configurations of the two elements. The distances between the elements and their position angle were then changed [Wnuk 2022a].

The configuration of the elements during the first measurement is shown in Figure 16, where the elements are arranged so that they are adjacent to each other with the side walls without gaps. During the measurements, the distance "a" between the elements was changed. Measurements were made for 0.7λ, 0.8 λ, 0.9 λ and λ, where λ = 10.7 cm for the center frequency f = 2800 MHz.

The measurement results are shown in Figure 17, where we can see that for all distances, the insulation between the elements decreases with increasing frequency. The elements definitely influence each other at a distance of 0.7 λ, from -17 db to about 24 dB. At the remaining distances, the value of the S_{21} coefficient ranges from -22 dB to -37 dB and they assume similar values with increasing frequency.

Correlation between the S_{21} coefficient distance occurs at three different operating band frequencies, see the characteristics in Figure 18. It is easy to notice that the nature of the changes in the insulation coefficient is very similar for all three frequencies under consideration.

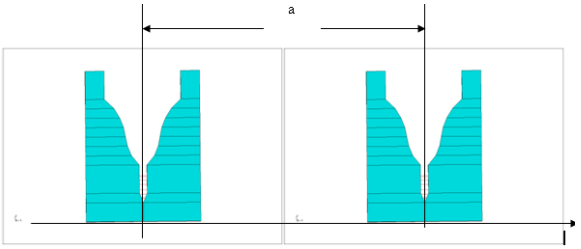

Fig. 16. Setting the elements for measuring the coupling between the antennas for different distances

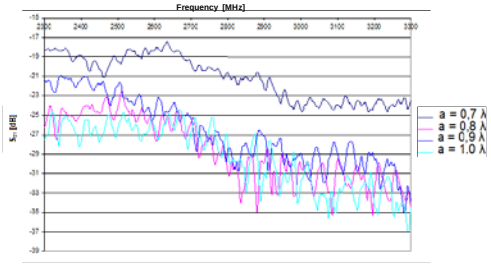

Fig. 17. Characteristics of the S_{21} coefficient for different distances between the antennas

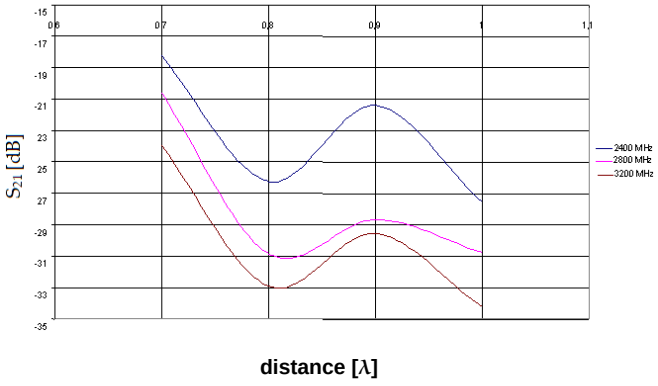

Fig. 18. Characteristics of the S_{21} coefficient for different distances between the antennas

The second measurement concerned the measurement of the S_{21} coefficient between the elements positioned as in Figure 16 and the adjacent walls with slots. The distance "a" between the elements 0.4 λ, 0.6 λ, 0.8 λ, and λ was changed during the measurements, where λ = 10.7 cm as in the previous case. The highest values of the S_{21} coefficient were achieved for the distance of 0.4 and 0.8 λ from -18dB

to -26dB, for the other two distances the achieved values are similar and are in the range from -21dB to -31dB. Figure 20 shows the change in the S21 coefficient depending on the distance between the elements for three frequencies of the operating band and, similarly to the previous case, shows that for the three considered frequencies the nature of the changes is very similar.

The third measurement concerned the positioning of the elements as shown in Figure 19; in this case, for the constant distance between the elements a = 0.5 λ, the angle of the elements relative to each other was changed, α = 30°, 60°, 90°. We can see a visible decrease in the value of the insulation coefficient for the angle of 90°, especially for the central frequency f = 2800 MHz, about -60 dB, for the remaining value of the α angle, the S_{21} coefficient reaches similar values ranging from -20 dB to -35 dB.

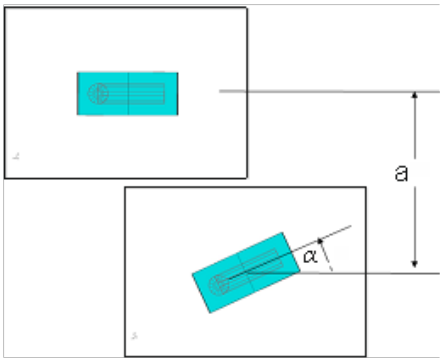

Fig. 19. Setting the elements for measuring the coupling between the antennas for different distances and for their different positions

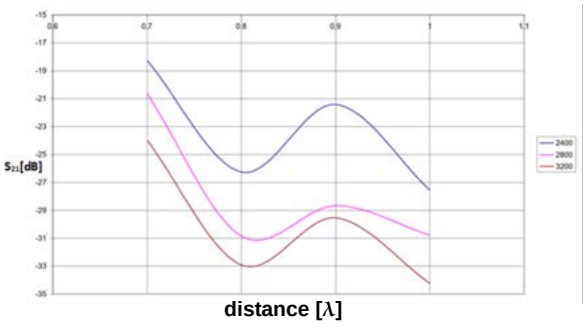

Fig. 20. Characteristics of the S_{21} coefficient for different distances between antennas

5. MEASURING THE CHARACTERISTICS OF THE DESIGNED PATTERN

This work item is devoted to measuring the radiation patterns of the antenna array, shown in Figure 22, composed of four adjacent TSA antennas, the structure of which has already been presented. The measurements were carried out for the E and H vector planes, as well as for the horizontal and vertical polarization, and the orthogonal polarization characteristics were measured.

The first measurement was to examine the characteristics in the vertical plane, the results of which are shown in Figure 24, which shows the radiation characteristics for all the tested frequencies, i.e. f = 2400, 2600, 2800, 3000 and 3200 MHz. The characteristics, apart from the orthogonal polarization, are standardized, but for a better visualization of the measurements, their description will be given for non-standardized values.

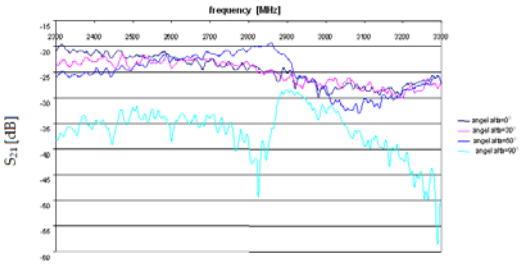

Fig. 21. Characteristics of the S_{21} coefficient for different positions of the antennas in relation to each other

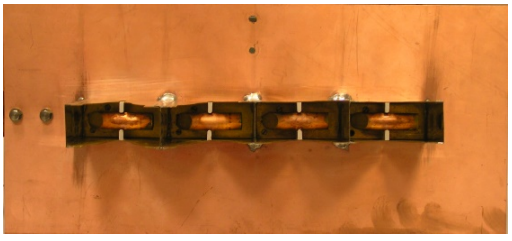

Fig. 22. The array of TSA antennas used to measure the radiation characteristics

The first measurement was to examine the characteristics in the vertical plane, the results of which are shown in figure 23, which shows the radiation characteristics for all tested frequencies, i.e. f = 2400, 2600, 2800, 3000 and 3200 MHz. The characteristics, apart from the orthogonal polarization, are standardized, but for a better visualization of the measurements, their description will be given for non-standardized values. For the characteristics at 2400 MHz, the maximum radiation is

at the level of -5.33 dB, the second maximum is at the level of -5.59 dB. The level of the first side lobe is about -27.17 dB, while the back radiation is -24.35dB. For the middle frequency of the operating band, the maximum radiation value is -5.56 dB, and the useful beam width at the half power level is 110.51°. The first side lobe has a level of -24.39 dB, and the reverse radiation is about -24.17 dB. The lowest level in the direction of maximum radiation is achieved by the characteristic for the frequency f = 3200 MHz and amounts to -8.15 dB.

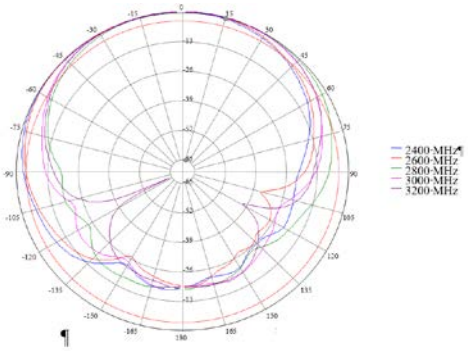

Fig. 23. Radiation characteristics for five different frequencies in the vertical plane

The beam width at the 3dB level is 104°, while for 4 dB it is approximately 113.72°. The back radiation level is -27.46 dB. The characteristics for all the frequencies are symmetrical. The next figures show the radiation characteristics in the vertical plane for orthogonal polarization.

Figure 24 shows the characteristics for all the measured frequencies, and it can be seen that they are all similar to each other. For vertical polarization the maximum radiation level is -5.56 dB, and for orthogonal polarization it is -27.45 dB. The signal was attenuated by about 21 dB.

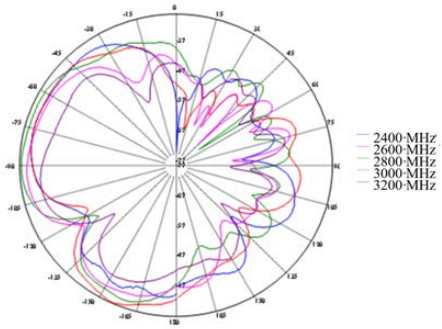

Fig. 24. Radiation characteristics for five different frequencies in the vertical plane for vertical polarization

The characteristic the maximum radiation obtained at a frequency of 2400 MHz is at the level of -5.8 dB. The useful beam width at the half power level is 34° and for 4 dB it is approx. 38°. The level of the first side lobe is about -15.25 dB, while the back radiation is -29.6 dB. For the central frequency of the operating band, the maximum radiation value is -5.61dB, and the useful beam width at the half power level is 23° (at 4 dB, the beam width is 26°). The first side lobe has a level of -17.31 dB, and the reverse radiation is about -36.64 dB.

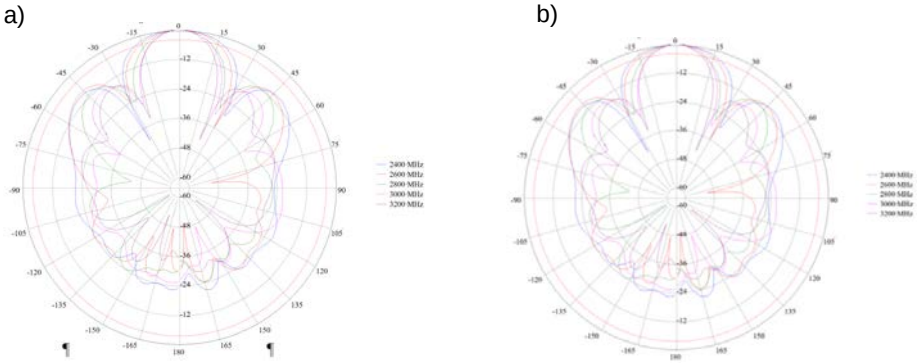

Fig. 25. Radiation characteristics for five different frequencies: a) in a horizontal plane, b) in a vertical plane

The lowest level in the direction of maximum radiation, similarly to the characteristics in the vertical plane, reaches the characteristic for the frequency f = 3200 MHz and amounts to -7.73 dB. The beam width at the 3 dB level is 19°, while for 4 dB it is about 23°. The back radiation level is -42.85 dB, and the first side lobe is -24.67°. All the characteristics are symmetrical.

The last two figures show the radiation pattern in the horizontal plane for orthogonal polarization. Figure 25a shows the characteristics for all the measured frequencies. Figure 2b5 shows the characteristic for the mid-band operation, as we can see in comparison to the characteristic at the same frequency in the horizontal plane (similar to the vertical plane) there was a significant attenuation of the signal. For horizontal polarization, the maximum radiation level is -5.56 dB, and for orthogonal polarization -31.8 dB. The signal is attenuated by about 26dB.

6. CONCLUSIONS

The article presents and analyzes the design, fabrication and testing of a single model of a TSA antenna with a widening gap and a linear array of antennas. The model of the TSA antenna, powered by a half-wave loop, is definitely a better solution than the model of the same antenna powered by a half-wave dipole, as is evidenced by the obtained results of the measurements of the SWR coefficient and radiation characteristics. The TSA antenna has the 0.87 [GHz] band (2.35–3.22 GHz) with the SWR < 2 value, and for SWR < 1.3 the 0.55 [GHz] band (2.50–3.05 GHz). The input resistance in the entire operating range is stable and has a value close to the value of 50 Ω. The radiation characteristics, both in the horizontal plane and in the perpendicular plane of a single element, are symmetrical characteristics, having no side lobes in the direction of the main radiation. The model of the TSA antenna is intended to work in an antenna array and will not be used as a standalone antenna. The radiation patterns are characteristics, and have greater directivity than a single element. Back radiation is additionally leveled with a screen located behind the power socket.

Obviously, it remains possible to design a TSA antenna model with a widening aperture, which is a continuation of the work with the existing TSA antenna design so that the new model achieves even more advantageous parameters, and the bandwidth is even wider and possible in a different frequency range. Searching for such a model should be based on changing the shape and dimensions of the slit and changing the type of wire that stimulates the slit.

In order to enable the design of another model of the TSA antenna based on the parameters of the already manufactured and ready TSA antenna, a detailed design algorithm in the WIPL-D environment has also been developed, which can be very helpful in creating, modeling and computer simulating the new designs of TSA widening-gap antennas (Vivaldi antennas). The obtained results will be used to estimate the plane array based on TSA antennas.

REFERENCES

Chen, X., Liang, J., Li, R., Guo, L., Chiau, C.C., Parini, G.G., 2005, *Planar UWB Monopole Antennas*, Microwave Conference Proceedings, APMC, Asia-Pacific Conference Proceedings, vol. 1.

Chio, T.H., Schubert ,T., Holter, D.H., 2000, *Characteristics of Dual-Polarized Tapered Slot Antena Array*, IEEE Transaction on Antennas and Propagation.

De Oliveira, A.M, Perotoni, M., Kofuji, B.S.T., Justo, J.F., 2015, *A Palm Tree Antipodal Vivaldi Antenna with Exponential Slot Edge for Improved Radiation Pattern*, IEEE Antennas Wireless Propagation Letters, vol. 14.

Frane, P.G., Leggetter, A.J., 1987, *Wideband Measurements on Vivaldi Traveling Wave Antenna*, IEE Proceedings, vol. 134, pp. 76–82.

Gazit, E., 1998, *Improved Design of the Vivaldi Antenna*, IEEE Proceedings H (Microwaves, Antennas and Propagation), vol. 135, pp. 89–92.

Gibson, P.J., 1979, *The Vivaldi Aeria*, 9th European Microwave Conference Proceedings, Brighton, UK, pp. 101–105.

Greenberg, K.L, Virga Hammond, C.L, 2003, *Performance Characteristics of the Dual Exponentially Tapered Slot Antenna for Wireless Communications Applications*, IEEE Transactions on Vehicular Technology, vol. 52, pp. 304–311.

Kolundzija, B.M., WIPL-D Ltd., *Electromagnetic Modelling of Composite Metallic and Dielectric Structures*, www.wipl-d.com/aboutus/aboutus.php.

Kołosowski, W., Wnuk, M., Jeziorski, A., 2023, *New Construction of Tapered Slot Antennas*, ICAP'2003, Exeter, UK.

Langley, J.D.S., Hali, P.S., Newman, R., 1996, *Balanced Antipodal Vivaldi Antenna for Wide Bandwidth Phase Arrays*, IEE Proceedings Microwave Antennas Propagation, vol. 143, pp. 97–102.

Li, M., Chang, Y., Li, Y., Dong, J., Wang, X., 2013, *Optimal Polarised Pattern Synthesis of Wideband Arrays Via Convex Optimisation*, IET Microwaves Antennas Propagations, vol. **7**(15), pp. 1228–1237.

Mikhnev, V.A, Vainikainen, P., 2006, *A Simple Tapered - Slot Antenna with Well - Matched Opening*, Poster on EuCAP Conference, Session 3PP4A.

Noronha, J.A.N, Bielawa, T., Anderso, D.G., Sweeney, D.G., Licul, S., Davis, W.A., 2003, *Designing Antennas for UWB Systems*, Microwave & RF, B.M.

Prasad, S.N., Mahapatra, S., 1983, *A New MIC Slot-Line Aerial*, IEEE AP-31, no. 3.

Schantz, H., 2005, *The Art and Science of Ultrawideband Antennas*, Artech House, Inc.

Schaubert, D.H., 1985, *Wideband Vivaldi Arrays for Large Aperture Antennas*, IEEE Transaction on Antennas and Propagation.

Slimi, M., Jmai, B., Dinis, H., Gharsallah, A., Mendes, P.M., 2022 , *Metamaterial Vivaldi Antenna Array for Breast Cancer Detection*, Sensors, vol. 22(10), pp. 39–45.

Valderas, D., Legarda, J., Gutierrez, L., Sancho, J.I., 2006, *Design of UWB Folded-Plate Monopole Antennas Based on TLM*, IEEE Transactions Antennas and Propagation, vol. 54, no. 6, pp. 1676–1687.

Wnuk, M., 2022, *Multilayer Dielectrically Periodic Antenna Structure in a Cascade View*, Applied Sciences, vol. 12, no. 9, pp. 1–14.

Wnuk, M., 2022, *Receiver Satellite Signal and Radio Locator Device in Band K*, Scientific Journal of Gdynia Maritime University, vol. 123, pp. 7–18.

Wu, F., Yuan, N., 2006, *The Radiation Characteristic of UWB Planar TEM Horn Antenna Array*, International Conference on Radar, CIE' 06, pp. 1–4.

Wu, X.H., Chen, Z.N., 2005, *Comparison of Planar Dipoles in UWB Applications*, IEEE Transactions on Antennas and Propagation, vol. 53, no. 6, pp. 1973–1983.

Zhao C.D., 2004, *Analysis on the Properties of Planar Dipole UWB Antenna*, Antennas and Wireless Propagation Letters, IEEE, vol. 53, no. 1, pp. 317–320.